The Atlantic Water Flow along the Vøring Plateau: Detecting Frontal Structures in Oceanic Station Time Series

J. Even Ø. Nilsen [a,b,c,*] and Frank Nilsen [b,d]

[a] *Nansen Environmental and Remote Sensing Center, Bergen, Norway*

[b] *Geophysical Institute, University of Bergen, Norway*

[c] *Bjerknes Centre for Climate Research, Bergen, Norway*

[d] *The University Centre in Svalbard (UNIS), Longyearbyen, Norway*

Abstract

The topographic steering of the baroclinic western branch of the Norwegian Atlantic Current (NwAC) determines the extent of Atlantic Water and location of the Arctic Front in the Nordic Seas. In this paper the geographical spread of hydrographic measurements at the Ocean Weather Station M (OWSM, 66°N 2°E) is utilised to create mean sections across the Vøring Plateau Escarpment in the Norwegian Sea. In concert with a theoretical framework involving the impact of low pressure systems on frontal jets over steep bathymetry, the behaviour of the front-current system at this location is described. It is shown that the halocline and thermocline are sloped from about 200 m in the west and down to 400 m in the east over 40 km centred on the station, indicating that the western branch of the NwAC is located here. The horizontal gradients introduced by this slope are 2°C and 0.1 for salinity. The frontal slope is not seen to change its inclination on seasonal, multi-annual, nor decadal timescales, indicating that the dynamic control of this frontal slope does not change appreciably. Further supported by the theoretical framework it is shown that the subsurface part of this front and the associated western branch of the NwAC is strongly locked by topography along the Vøring Plateau also on short timescales. From large scale bathymetry it is also shown how this kind of frontal locking can be expected over most of the ridges and continental slopes in the Nordic Seas.

Key words: Fronts, Atlantic Water, Nordic Seas, Ocean Weather Station M, topographic effects, baroclinic motion, 15°W–15°E, 60°N–70°N

* Corresponding author. Tel: +47 55205881; fax: +47 55205801.
Email address: even@nersc.no (J. Even Ø. Nilsen).

1 Introduction

By definition, fronts are regions of large horizontal gradients of certain properties, usually including density. Fronts are marked by large thermocline/halocline slopes, large in the sense that the depth variation of an isotherm/isohaline across a front is typically on the order of the isotherm/isohaline depth itself. From this point of view it should be emphasized that an oceanic front is identified not only by a sea surface property gradient, but more importantly by its subsurface slope. Whereas the surface part of the front might be influenced by shallow surface processes, such as the development of the seasonal pycnocline and Ekman transports, the deeper and larger part of the front remain governed by the dynamics of its associated baroclinic flow. In the Nordic Seas the cold, fresh Polar Waters, the warm, saline Atlantic Water (AW), and their mixing product, the Arctic Water, residing mainly in the Greenland and Iceland Seas, produce such large thermocline and halocline slopes between them (representing large pycnocline slopes and thus producing dynamical effects). These are called the Polar Front and Arctic Front (AF), respectively (Swift, 1986).

The topography and AW surface currents in the Norwegian Sea are shown in Figure 1. Ocean Weather Station M (OWSM, 66°N 2°E) is situated over the steep slope from the Vøring Plateau down to the Norwegian Basin floor. The hydrography and variability in this area have been thoroughly described by Nilsen and Falck (2006), and the whole Nordic Seas' oceanographic features are reviewed by Blindheim and Østerhus (2005). In this paper we will focus on the AF in the Norwegian Basin and the related current. The current system of the Norwegian Atlantic Current (NwAC) is considered to be a two-branch system with a topographically controlled barotropic current along the Norwegian continental slope and a baroclinic jet following 2000–2500 m isobaths (Mork and Blindheim, 2000; Orvik et al., 2001; Orvik and Niiler, 2002). At the Svinøy Section, the western branch is identified as a 400 m deep and 30–50 km wide frontal jet (Orvik et al., 2001). This jet is connected to the subsurface part of the southeastern part of the AF, the Atlantic Norwegian Front (ANF; Szczechowoski, 1994; Smart, 1984) [1] .

The AW is spread over the whole area between these two current branches, and to a certain extent outside but then at shallower depths. This spreading is due to extensive eddy activity (Sælen, 1963; Rodionov, 1992) and atmospheric

[1] Smart (1984) uses the name Norwegian Current Front, but the potential for confusion with the Norwegian Coastal Current makes Szczechowoski's (1994) naming more suitable. Note also that the Jan Mayen Front, separating the waters of the Iceland Sea and the predominantly recirculated AW in the Norwegian Basin (Read and Pollard, 1992), sometimes is considered the AF in this area, but our focus is on the NwAC and thus on the ANF.

forcing. The surface distribution of AW varies considerably with season and other atmospheric influences (Blindheim et al., 2000; Furevik et al., 2002; Nilsen and Falck, 2006). The NwAC is often characterized as a wedge shaped "current". However, already from the early measurements of Helland-Hansen and Nansen (1909) it was clear that the lower boundary of the AW (35.0 isohaline) spreads in an uneven fashion, but horizontally on average, as far as the 2000 m isobath before showing any persistent upward sloping (see Figure 2). The severe vertical displacements of this boundary, first referred to as "puzzling waves" by Helland-Hansen and Nansen (1909), are elaborated upon thoroughly by Dickson (1972). They are most likely explained by the existence of large eddies in the inflowing AW (Sælen, 1963), although the alternative explanations, such as internal waves (Krauß, 1958) and "sudden variations in the velocity ... of the surface currents" (Helland-Hansen and Nansen, 1909), can be viewed as different formulations of the same dynamics.

The upward westward sloping of isotherms and isohalines at 2000 m water depth is characteristic of most sections across the NwAC (e.g. Figure 2). The AW entering between Iceland and the Faroes forms the clearly defined sloping Iceland–Faroe Front against the colder and fresher waters of the Icelandic and western Norwegian Seas (Hansen and Østerhus, 2000). North of the Faroes the AW enters the southeast Norwegian sea as the Faroe Current along the Faroese continental shelf break. The Sognefjord Section cuts across the bottom of the ridge from the northeast corner of the Faroe Plateau, and here the front is clearly visible NW of the ridge (Helland-Hansen, 1934; Sælen, 1959). Over the weak bottom slope further north, at the Svinøy Section, the mentioned unstable baroclinic frontal jet is located approximately above the 2000 m isobath (Leinebø, 1969; Mork and Blindheim, 2000; Orvik et al., 2001). Such a front is also seen in the 6S Section along 65°45'N (Borovkov and Krysov, 1995; Anon., 1997; Blindheim et al., 2000) from which the three years 1996–1998 are shown in Figure 3. Hydrographic surveys of the area around and south of the Vøring Plateau in 1935, '36 and '65 (Mosby, 1959, 1970; Bjørgen, 1971), show highly variable hydrography, both in time and space, and the existence of eddies. But the outer slope of the AW interface and calculated geostrophic surface current maxima most often coincide with the position of OWSM. Across the Vøring Plateau at the latitude of OWSM (66°N) mostly sporadic measurements have been done, the most focused on this area being the Anglo-Norwegian Variability Project during seven weeks in the spring of 1967 (Kvinge et al., 1968). Dickson (1972) studied the waviness of the isolines in these 17 sections and a few others and found that the frontal slope at OWSM was the most pronounced and persistent feature here. Other sections along 66°N are shown in Gammelsrød and Holm (1984).

Another type of spatial study in this area are AXBT (Airborne Expendable Bathythermograph) surveys from January 1980 to July 1981 (Smart, 1984). This dense dataset, covering all seasons, reveals the ANF at around 200–400 m

depth, following the 2000 m isobath along the Vøring Plateau Escarpment with a lateral variation in position as small as about 50 km. He also observed that the steepness of the frontal slope did not appear to be seasonally dependent, but the slopes did show regional dependence on the local steepness of the bottom topography. All the above mentioned surveys indicate a sloping interface between AW and Arctic Intermediate Water, above the same isobath as the one below OWSM.

That the surface current in the western branch of the NwAC follows the frontal structure is shown by drifters (Poulain et al., 1996; Orvik and Niiler, 2001). These drifters show the swiftest surface currents to follow the steepest bottom slopes and the clearest separation of the two branches of the NwAC to be across the Vøring Plateau. Using a two layer model Heburn and Johnson (1995) show a clear dependence on topography for the circulation, but they do not resolve the two branch structure of the NwAC very well. Using particle tracking in the Princeton Ocean Model (POM) Hjøllo (1999) clearly demonstrate a tendency for most of the Atlantic Water in the Faroe Current to follow the 2000 m isobath towards and along the Vøring Plateau slope.

Note that the existence of a frontal structure at the position of OWSM has implications for the interpretation of variability in the time series. This was early recognized by Mosby (1950), who showed a variation of the depth of the transition layer with as much as 300 m in chosen profiles taken within a week of each other. Later studies of OWSM data also hold forth perturbations of the sloping frontal structure as an explanation for rapid changes in the hydrographical records (Le Floch, 1953; Mosby, 1959; Johannessen and Gade, 1984; Gammelsrød and Holm, 1984). Varying ship positioning (demonstrated in the next section) may have similar effects, but Gammelsrød and Holm (1984) found no systematic variability or correlations with the hydrographic data.

The literature reviewed here indicates that the baroclinic western branch of the NwAC and its associated subsurface front are guided by topography. The question remains, however, whether this is true for all timescales. Also of key importance is the effect of steep topography like the Vøring Plateau Escarpment on locking of fronts (as found by Smart, 1984), relative to weaker bottom slopes. For instance, in the southeastern Norwegian Sea the whole vertical structure of the ANF has been observed to move laterally (Furevik et al., 2002).

In this paper we will focus on the Vøring Plateau and address these questions by using a long time series in concert with theoretical considerations. First, the geographical spread of hydrographic data from OWSM will be utilized to identify and study the characteristics of the sloping pycnocline, both for the overall mean and for different time periods (Section 3.1–3.4). Then the front's

persistence over the bottom slope and the mechanisms behind will be assessed by relating the results to a theoretical framework involving atmosphere-ocean interaction (Section 3.5–3.6). The main goal is to assess whether and how this subsurface front is locked to the bottom slope from the Vøring Plateau.

2 Materials and Methods

Figure 4 shows the distribution of all the measurements taken at OWSM between 1948 and 1999. The measurements of temperature and salinity are taken around the standard depths of 0, 10, 25, 50, 75, 100, 150, 200, 300, 400, 500, 600, 800, 1000, 1200, 1500 and 2000 m, using Nansen bottles equipped with reversing thermometers. The program carried out at the station consists of daily casts down to 1000 m, and weekly down to the bottom (Gammelsrød et al., 1992). Counting every single sample (not profiles), the dataset consists of some 94 000 values of each variable. As can be seen, the precision in positioning has not always been perfect. Note also that the spread of measurements roughly covers the whole escarpment. After the creation of a Cartesian coordinate system with origin at 66°N 2°E and rotated 17° anticlockwise (Figure 5a), it is possible to study the spatial distribution of the samples (Figure 5b,c). The system's alignment is based on the assumption that a topographically steered jet will follow the topography, and that the associated sloping front can be found by studying a section perpendicular to the escarpment. The exact choice of rotation angle is based on minimization of the hydrographic gradients along the y-axis, and this makes the coincidence with the isobaths (Figure 5a) a strong indication that the front is aligned with the escarpment. The samples are almost normally distributed, and the bulk of data are found inside a ±20 km interval in both directions (Figure 5b,c). The variation in time of the deviation from 66°N 2°E can be seen in Figure 6, and the largest spread is found in the beginning of the series and during the 1970s.

For calculation of an overall mean section, the cross-slope section was divided into nine 10 km wide bins laterally and 17 bins centred on the standard depths (Figure 7). All samples in time and y-direction falling inside a bin form the basis for the mean value for this bin. The section along the escarpment (y-direction) was created in the same manner.

The temporal inhomogeneity of the sample spread (Figure 6) has implications on this spatial study, in that any values calculated for far away locations will be based on data only from these specific periods in time. The number of profiles in the outer bins (at 40 km) are around 70 increasing to more than 1500 at 10 km and 5000 at the centre (Figure 5b). Their total count being relatively low, the outer bins reflect the overall temporal distribution with most samples during the 1950s and 1970s (not shown). Strictly speaking,

from this the only bins with appreciable temporal homogeneity are in the 5 central columns (± 20 km, see Figure 6). The annual distribution of samples on the other hand, is homogeneous in all bins. The error estimate for the mean values (s_m) is calculated following

$$s_m^2 = \frac{s^2}{n}, \tag{1}$$

where s is the estimated standard deviation, and n the number of samples in the bin.

In addition to the overall mean sections, differences between the four seasons and between high and low phases of the North Atlantic Oscillation (NAO) are studied by cross-slope sections of bin-means from the same dataset. Because of the reduction of sample number in this temporal separation, and the scarcity of data far from 66°N 2°E, the width of the sections had to be reduced to 40 and 20 km respectively. But given the large amount of samples within these distances of the station position, it was possible to increase the resolution of the sections to bin sizes of 4 km and 2.5 km.

In this work we use only hydrographic data from OWSM, since our intention for a large part is to show how a time series station can be utilized for spatial studies. To use other sections from ∼66°N to better the statistics for the marginal parts of our study might have been possible, but being sporadic, available sections are not likely to provide significant gain regarding the long-term aspects of our work. However, a case study will be made of the 6S-Sections shown in Figure 3. Use of other data sources is more relevant for a wider study of the Norwegian Sea and thus reserved for future work.

3 Results and Discussion

3.1 Overall Mean Sections

The resulting cross-stream mean salinity section is shown in Figure 8a. The section shows a halocline sloping from about 200 m in the west and down to 400 m in the east. There is also a fresher surface layer, which is related to the fresher shallow summer mixed layer in this area (Nilsen and Falck, 2006). The mean sections of temperature (Figure 9a) show the same characteristics, with warmer water above and to the east and a sloping thermocline at the same depths as the halocline. The frontal slope gives mean horizontal gradients of 0.1 in salinity and 2°C over 40 km at these depths. The frontal structure is present in both salinity and temperature, so it can be expected to be for

density also. Still, since the density distribution determines the dynamics of a system, a density section is shown in Figure 10.

The sections (y) along the escarpment (Figures 8b–10b) show a distinctly more flat structure, with small or nonexistent horizontal gradients. There is a slight upward tilt in isotherms and isohalines toward the south, and the possible dynamical explanation for this lies in the eastward bend in the isobaths south of OWSM (Figure 5a) which a topographically controlled front will tend to follow. The contrasts between the two perpendicular sections leave no doubt that the mean situation involves a frontal structure aligned with the escarpment.

Also embedded in the plots (Figures 8–10) are error estimates given by (1) in white contours. These show the most unreliable mean values to be near the edges of the sections as expected due to the scarceness of data here. But within 20 km of the middle position, the errors are less than 1/10 of the contour intervals used to plot the property. This means that the patterns seen are reliable. The variance within the bins (i.e., the distribution of variance over the section) is shown with black contours. These show the strongest variance focused along the strongest gradients, and the interpretation of this will be discussed later.

3.2 Seasonality

The two branches of the NwAC react differently to the changes of seasons. In the Faroe Current, the saline AW is more widely distributed in summer than in winter (Hansen et al., 2000), and Mork and Blindheim (2000) found that the core of AW furthest offshore at the Svinøy Section is less distinct in the winter and spring. To investigate the horizontal characteristics and the frontal behaviour across the slope over the year, the data from OWSM was divided into four seasons using the same months as Hansen et al. (2000), and mean sections for the three water properties were created.

The salinity sections reveal a broader, somewhat deeper, and more saline core in the summer (Figure 11b and c). This can be due to the seasonal signal in AW flow in the western branch of the NwAC. There is also an apparent horizontal shift in the Atlantic water masses, but the fresher AW column in the early winter is not necessarily caused by lateral movements of the NwAC. Instead the salinity cycle is more likely to be caused by vertical mixing in autumn of the fresh summer layer seen in Figure 11b and c. This layer originates mostly from the Norwegian Coastal Current and enters as Ekman transports in the shallow summer mixed layer (Nilsen and Falck, 2006).

The temperature sections in Figure 12 do not show any large horizontal differences between the seasons, and this is due to the atmospheric heat fluxes'

dominant influence on the temperature in the upper waters. The density section (Figure 13) shows the strong stability of the warm and fresh summer mixed layer near the surface, but since the density variations in the upper water masses at OWSM are almost entirely determined by temperature variations, there is no sign of the lateral structure seen in the corresponding salinity sections.

The more interesting result from these seasonal sections with respect to the question of frontal locking is that the frontal slope (slope of the halo-, thermo- and pycnocline) is similar through all seasons. That is, not only is the slope roughly constant, which alone would not tell us anything about lateral shifts, but the depth of the front in the middle of the section is also the same. Note that this does not exclude variability in frontal position on timescales other than the seasonal, but, given the generally strong variability the annual cycle represents, this is an important result.

3.3 Relation to the North Atlantic Oscillation

Mork and Blindheim (2000) found that the temperature and salinity in the western part of the Svinøy Section are negatively correlated with the NAO-index. Studies of the distribution of AW in the surface layers across the Norwegian Sea also show a wider (westward) spread of these waters some 2–3 years after periods of low NAO winter index, and a narrower surface signature after high index periods, attributed to changes in the pathways into the Nordic Seas (Blindheim et al., 2000). Supporting this, a model study by Nilsen et al. (2003) shows a long-term anti-correlation between the inflow on each side of the Faroes. This correlation is related to the NAO so that during high index years the eastern branch of the NwAC receives more AW from the North Atlantic than the western branch.

The OWSM-data from winters (Dec–Apr) in longer periods of relatively high ('73–'76, '81–'84, '89–'95) and low (i.e. weak or negative, '68–'72, '77–'80, '85–'88) winter NAO-index (Figure 14) were separated to make corresponding mean sections. The results in Figure 15 show that also at OWSM there are changes related to these time periods. The salinity sections (Figure 15a) show the same relation to the NAO-index as cited above, with a fresher Atlantic layer in high index years than in low, at this location. In the high index situation, the most saline waters are found in the eastern part of the section, i.e. there is a stronger lateral gradient in the upper waters. This horizontal shift in water mass characteristics in the AW seems to tilt the isohalines down to the east of OWSM and consequently strengthen the horizontal gradient in the frontal slope as predicted by Nilsen (2001). This also corresponds to the results of Blindheim et al. (2000). In the periods where the surface front in salinity is found close to the eastern side of the Norwegian Basin, sections

from OWSM show the same eastward shift, and vice versa for the periods with widely spread AW in the basin. Lagging our periods by the suggested 2 years (not shown) yielded even clearer differences in salinity, supporting the findings of Blindheim et al. (2000).

It is hard to discuss these results in terms of NAO impact, since the chosen periods are long and prone to be influenced by long term variability. Occurrence of events like the Great Salinity Anomalies (Belkin et al., 1998; Dickson et al., 1988; Belkin, 2004) and the fact that the 1960s was a period of high salinity both at OWSM and in the return flow on the western side of the basin (Alekseev et al., 2001) influence the interpretation of the results here as well as those of Blindheim et al. (2000). Independent of their causes, it is interesting to set the two clearly different situations in contrast to each other, in order to see if these changes in water mass distribution have any impact on the frontal structure (i.e. density gradients). In the same manner as between the seasons, the temperature (Figure 15b) does not show any significant changes between high and low NAO periods, and thus the calculated density structure was not found to be significantly affected by the winter NAO-index either (not shown).

3.4 The Pycnocline Slope and Variability

Up to this point, the question whether the ANF is locked above the steep Vøring Plateau Escarpment has only been qualitatively addressed using Figures 8–13 and 15. Apart from the changes in water mass distribution in the upper waters, all the cross sections seem to have a similar slope in the different properties.

The most important of these properties for localizing the front and position of the baroclinic jet is density. In Figures 8–13 and 15, the isopycnal of σ_t=27.8 is plotted as representative of the frontal slope. In addition to the cases already shown, a separation between periods of basin wide and limited spread of AW from the NwAC according to Blindheim et al. (2000) was done (as expected, this showed basically the same salinity distributions as for the NAO-study in Figure 15a, only with an even clearer difference). Isopycnals of σ_t=27.8 for all these cross sections are gathered in Figure 16a. The isopycnal slopes show a frontal structure basically indifferent to the changes in upper layer water properties inferred by the annual cycle and the interannual to decadal variability in phase with the NAO. The steepest part of the frontal slope deepens from 280 to 400 m depth over 40 km centred on OWSM. The lateral spread of curves from the different situations are only on the order of 4–8 km in the range of appreciable amounts of data (±10 km). More importantly, the spread consists of random irregularities in each slope rather than a discernible separation of slopes. Any separation or difference in steepness of slope fall inside this range

of noise. The details in the seasonal slopes outside the ±10 km range cannot be given any significance because of the scarceness of data there. Thus if the part of the frontal slope encompassed by these sections is representable or at least part of the front, difference in the baroclinic current speed in the western branch of the NwAC between high and low NAO periods or in an annual cycle is not likely.

On longer time scales, however, isopycnal depth has been observed to vary at OWSM (Nilsen, 2003). To study the cross section signature of this, mean sections for the last five decades have been produced (not shown) and the pycnocline slopes are plotted in Figure 16b. The depth of these isopycnals show a sloping isopycnal at varying depths: In the 1950s approximately 20 m shallower, in the 1970s deeper by almost the same amount, while in the other decades close to the mean. The steepness of the slope does not change because of the long term changes. Note that the use of the term "depth" in relation to the sloping isopycnals in Figure 16 is somewhat inappropriate since no levelling is seen at the ends of the slopes and a "deepening" might translate as a westward shift. It is not possible from these data to distinguish between the two, although it will be argued that the frontal slope has fewer degrees of freedom laterally because of the topography than it has vertically where changing water mass characteristics may alter the structure of the water column. Consequently, these results indicate that the decadal variability in hydrography is not followed by changes in the baroclinic velocity of the western branch of the NwAC.

Short term variability is hard to isolate from composite studies of these data. As already shown, separating the dataset into subsets strongly limits the lateral extent of spatial studies from station time series. The fact that the sloping front has a mean position as shown in the different sections does not exclude the possibility of lateral excursions. Horizontal gradients in the mean sections will be somewhat smoothed by lateral movements and other changes in the front, but a mean gradient will still be present.

However, short term variability in the hydrography near a front is most often connected to movement of (the strong gradients in) the front. A front that spends just as much time away from its mean position as in the middle of it will leave a broad area of variability, while short-term variability on an otherwise stably positioned front leaves a more concentrated band of variance. Thus the frontal slope can be localized by maxima in variance, and in Figures 8–13 and 15 the variance within the bins (i.e., the distribution of variance over the section) is shown with black contours. All sections have variance maxima focused on the sloping front. The presence of a variance maximum around the front is not unexpected, but their slanted character and narrowness relative to the gradient of the property indicate that frontal excursions from the mean position are limited. This localisation of a frontal structure and variability

maxima is also shown by Dickson (1972, his Figure 136) in a study of 17 consecutive sections along 66°N. The maximum range of T and S between these sections is found to be focused not only along the pycnocline (as expected), but also at two lateral maxima, namely along the sloping part of the pycnocline (under OWSM) and at the interception with the continental slope. The latter is merely the result of a stronger gradient there, while the former is connected to the existence of a persistent isopycnal slope at this position. Dickson's (1972) results confirm the frontal locking during that particular cruise period, while our results indicate that this is true also on long time scales.

3.5 The Barotropic Assumption

Now that the results from OWSM have been presented and indications of a stably positioned frontal slope have been pointed to, we will present a theoretical framework explaining the locking of a baroclinic front over a deep bottom slope. Through this section and the next, theory will be presented and the results from OWSM will be further discussed.

Willebrand et al. (1980) found that a forcing function with scales much larger than O(100 km) and periods between the inertial period and ∼300 days induced oceanic motion that was depth-independent (barotropic response), the baroclinic part being a direct local response to the Ekman pumping. The oceanic response to large-scale forcing can differ strikingly from this if the bottom topography is taken into account. Then the horizontal length scale L is determined by the slope width, and the scales of forcing and ocean response are no longer directly related. As discussed by Willebrand et al. (1980), the answer to the question whether or not the flow will be baroclinic now depends on the topographic as well as the atmospheric scale. If the atmospheric scale is assumed to be much larger than that of topography, the wind-induced barotropic flow produces a vertical velocity field at the bottom, which has the same scales as the topography. This vertical velocity field can induce either an additional barotropic signal or a baroclinic motion trapped near the bottom. It can be determined which of the two is occurring by using the Burger number:

$$B(z) = \frac{\left(\frac{N(z)D}{f_0}\right)^2}{L^2} = \left(\frac{R_i(z)}{L}\right)^2, \tag{2}$$

where N is the Brunt-Väisälä frequency, D is the characteristic depth, f_0 is the local Coriolis parameter, and R_i is the internal Rossby radius of deformation. If $B \ll 1$, the stratification will be less important, and the flow field is predominantly barotropic.

The barotropic response of the ocean is described by the vertically integrated equations of motion. Although the water column stratification is highly baroclinic at OWSM and along the slope from the Vøring Plateau, investigation of topographically trapped waves can be done by means of a barotropic or homogeneous model including friction. The underlying assumption is that the internal Rossby radius of deformation is much smaller than the characteristic horizontal length scale (Rhines, 1970). Thus the effect of topography during the spin-up phase is felt mainly by the barotropic mode. The dominant frequencies which will be observed during the spin-up of a baroclinic ocean are almost exactly those of the purely barotropic modes (Rhines, 1970; Anderson and Killworth, 1977; Nilsen, 2004). The focus on the spin-up phase is due to the fact that the spatial wind stress field over the Norwegian Sea is highly fluctuating: As soon as a low-pressure centre has started to get a hold of the water column, it either moves away from the area and free oscillations are released, or it is replaced by a new pressure centre and spin-up starts again.

Measurements at OWSM (e.g. Figure 10) and from the Russian section along 65°45'N in the Norwegian Sea (6S; Figure 1; Borovkov and Krysov, 1995; Anon., 1997; Blindheim et al., 2000) show that the water column can be approximately represented by a two-layer model with an upper layer thickness between 200 and 400 m in the winter and spring (Figure 3 and Figure 13). The Rossby deformation radius for a two-layer model with an upper layer H_1 and a lower layer H_2 is given by

$$R_i = \frac{c_i}{f_0}, \quad c_i^2 = g\frac{\rho_2 - \rho_1}{\rho_2}\frac{H_1 H_2}{H_1 + H_2} = g'\frac{H_1 H_2}{H_1 + H_2}, \tag{3}$$

where c_i is the phase speed for the baroclinic wave, and g' is the reduced gravity. Using the mid-depth of the sloping bottom as the characteristic water depth, i.e. $D = H_0 = 2250$ m, $H_1 = 400$ m, $\rho_1 = 1027.6$ kg m^{-3}, $\rho_2 = 1028.1$ kg m^{-3} and $f_0 = 1.33 \cdot 10^{-4}$ s^{-1}, (3) results in c_i=1.3 m s^{-1} and R_i=9.7 km. Thus for a horizontal scale of 73 km, which is the characteristic width of the Vøring Plateau Escarpment (Nilsen, 2001), stratification will play a marginal role in the spin-up phase since $B \sim 0.02$ when (3) is used in (2). Based on the results in Nilsen (2004), where it is shown that the forcing by the variability of the pressure systems over the Vøring Plateau can be represented by a wave length on the order of the Vøring Plateau Escarpment length, the barotropic mode is assumed to be the dominant mode in the spin-up phase.

Figure 17a shows the wind stress curl calculated from the wind stress vectors (Figure 17b) over the Nordic Seas and the Barents Sea as a response to a low-pressure system over northern Norway and the western Barents Sea. This was one of the largest negative curl events over the Vøring Plateau in 1997, and it lasted long enough for the calculated Ekman pumping to raise the water column above the Vøring Plateau Escarpment by ∼1 m. The curl field forcing

function (Figure 17a) acting on our study area was relieved by a positive curl field a couple of days later (Nilsen, 2001), and Figure 17c shows that the wind stress curl field contains significant oscillating energy on the wave period band between 50 and 200 h. These oscillations are important in the spin-up phase for topographically trapped waves.

3.6 Forced Waves and Spin-up

Here we will characterize the forced water column and spin-up phase through the quasigeostrophic potential vorticity (QPV) equation. A rigid lid approximation is used, and the effect of viscosity on the interior is neglected. The lateral diffusion of vorticity is also neglected by assuming the Reynolds number $Re \to \infty$ in the interior. The topography dominates over the β-effect (Nilsen, 2004), and thus a constant Coriolis parameter is used. By these approximations and linearizations, the QPV-equation for a barotropic response of the ocean to a wind stress is described by

$$H\frac{\partial}{\partial t}\left(\nabla\cdot\frac{\nabla\psi}{H}\right)+f\frac{H_x}{H}\frac{\partial\psi}{\partial y}=\frac{1}{\rho_r}\vec{k}\cdot(\nabla\times\boldsymbol{\tau})=C(x,y,t), \tag{4}$$

where $H = H(x)$ is the depth across the Vøring Plateau slope, $H_x = dH/dx$, $\boldsymbol{\tau}$ is the wind stress vector, and ψ is the volume transport stream function defined so that

$$Hu=-\frac{\partial\psi}{\partial y},\quad Hv=\frac{\partial\psi}{\partial x}. \tag{5}$$

The transformation $\psi = H^{\frac{1}{2}}\varphi$ in (4) yields

$$\left(\nabla^2-V(x)\right)\frac{\partial\varphi}{\partial t}+f\frac{H_x}{H}\frac{\partial\varphi}{\partial y}=\frac{C}{H^{\frac{1}{2}}}, \tag{6}$$

where

$$V(x)=H^{\frac{1}{2}}\nabla^2H^{-\frac{1}{2}}. \tag{7}$$

$V(x)$ is identified as the potential function of the topography, described more in detail by Nilsen (2001). Equation (6) can be viewed as an advection equation for the wave form φ forced by the expression on the right hand side. The wave form is advected along the y-direction, i.e. along the escarpment. In the absence of the forcing term, the fraction $f\frac{H_x}{H}/\left(\nabla^2-V(x)\right)$ can be interpreted

as a phase speed for the topographically trapped wave propagating in the y-direction.

An important fact from (6) is that, for waves over topography, $f\frac{H_x}{H}$ takes the role of β for planetary waves. The magnitude of this term determines how apparent these waves will be in the area of interest, and also what horizontal length scale these waves will have. Plotting the reciprocal of $\frac{H_x}{H}$, based on the ETOPO5 bathymetry for the Nordic Seas, reveals where there most likely will exist topographically trapped waves and what their horizontal scales will be (Figure 18).

As shown in Figure 17 and by Nilsen (2004) the wind stress curl over the Vøring Plateau slope can contain high level energy on the period interval between 48 and 185 h. The forcing term in (6) can be represented by a forcing function constructed as a sum of (infinitely) many Fourier components, and Nilsen (2004) reported that if this forcing function contained variability corresponding to a wave length of ∼76 km and an oscillating period of ∼100 h, a resonant response for topographically trapped waves can occur over the slope. These are also the characteristic length and time scales for the Vøring Plateau slope around OWSM (Nilsen, 2004). Thus the following explanation for locking of the frontal structure over the sloping sea floor can be given: The larger variability in the wind stress curl is a result of strong atmospheric pressure systems traversing the Nordic Seas. If the wind stress curl field contains variability corresponding to the length and time scales supported by the Vøring Plateau slope, the response will primarily be a barotropic perturbation of the water column. Hence information of a sloping ocean floor is communicated to the dynamics in the whole water column. Pressure systems over the Vøring Plateau are soon replaced by new strong pressure systems, and thus the spin-up process starts over again with a possible barotropic response. Although these perturbations can initiate current meandering and eddy formation they also serve to trap the frontal and current system above the slope (Nilsen, 2004).

A case for such air–ocean interaction can be made by comparing the 6S sections from 1996–1998 (Figure 3) with the time series of wind stress curl variance in the 50–200 h period band for the same years (Figure 17c). The three CTD sections (Figure 3) are collected across the Vøring Plateau in the beginning of June each year. The front is locked above the slope every year, but the temperature and salinity contours seem to be more vertically displaced in 1997. This could be due to the maximum in curl variance occurring later in 1997 than in the other two years, as shown by the 6-month average in Figure 17c. Snapshots of the extreme forcing situation in May 1997 are shown in Figures 17a and b, and the undulating isotherms and isohalines the next month (Figure 3) could be the signature of long lived current-meandering and eddies along the Vøring Plateau Escarpment.

From the theory presented here, higher variance in the density field is expected for years with large time variability in the wind stress curl field and is therefore a signature of a higher degree of frontal trapping. In the temperature and salinity data from OWSM, such an increased variance in the frontal area is found for the winter months (Figure 13a and d) relative to the rest of the year, and in high relative to low NAO-index winters (Figure 15). Thus these cases correspond to the increased activity of low pressure systems traversing the Nordic Seas and indicate stronger frontal trapping also on shorter time scales.

Since the time resolution for our mean sections is rather coarse, we are not able to study the spin-up phase of topographically trapped waves. We have to turn to the time averaged versions of the above theory and physical explanations. Nøst and Isachsen (2003) show that there is a northward geostrophic bottom current along the Vøring Plateau slope, created or "forced" by the averaged wind stress curl field through Ekman pumping. A topographically steered mean abyssal current can in turn steer upper ocean currents with the surface current bending in the direction of the abyssal current. By using a simple two-layer geostrophic model with an active lower layer Svendsen et al. (1991) showed in a very clear and direct fashion how abyssal currents $\vec{v_2}$ can steer upper ocean currents. The current $\vec{v_1}$ in the upper layer becomes

$$\vec{k} \times (\vec{v_1} - \vec{v_2}) = g' \nabla H_1. \tag{8}$$

As mentioned, the area around the ANF is influenced by eddies shed from the front and meanders of the front itself (Rodionov, 1992). However, the current field is observed to reestablish after perturbations and thus have a quasistationary character (Kort et al., 1977). Thus the long-term current pattern will obey the topographic control.

4 Conclusions

In this paper we have identified the sloping Atlantic Norwegian Front over the Vøring Plateau Escarpment by utilizing the spread of data from Ocean Weather Station M. The use of profiles from a single station to create spatial sections of hydrography is shown to be applicable for producing long term mean sections as well as composite studies.

The sections from OWSM show a thermocline and halocline sloping from about 200 m in the west and down to 400 m in the east over the 40 km covered, with warmer and more saline waters above and to the east. The resulting horizontal gradients (0.1 for salinity and 2°C over 40 km) are considerable for a 50 year mean field.

Seasonal sections reveal a broader and stronger salt core in the summer, supporting the findings of more saline and widely distributed AW near the western branch of the NwAC (Hansen et al., 2000; Mork and Blindheim, 2000). Composite sections from periods with high and low winter NAO-index show that at OWSM there is a more wide (westward) distribution of AW during periods of low NAO-index, coherent with the findings of Blindheim et al. (2000) and Mork and Blindheim (2000).

A more central result is that despite these hydrographic changes the position of the frontal slope is not seen to change. And on decadal timescales, for which the depth of the slope varies, no change is seen in frontal steepness. This indicates that although the hydrographic conditions in the water column and the neighbouring waters change, the dynamical control of this frontal slope and the velocity of the western branch of the NwAC do not change appreciably on timescales from seasonal to decadal.

Regarding the short-term behaviour of a topographically locked baroclinic current, a physical explanation is presented through the quasigeostrophic potential vorticity equation. It is argued that when the variability of the wind stress curl field contains the length and time scales supported by the bottom slope, the response will primarily be a barotropic perturbation of the water column. Hence information of a sloping ocean floor is communicated to the dynamics of the whole water column. Although these perturbations can initiate current meandering and eddy formations they also serve to trap the frontal- and current system above such a slope.

For our study at the Vøring Plateau escarpment the theory is supported by the variance field in the cross sections from OWSM-data. Firstly, the focused variance around the mean frontal slope indicates limited excursions from the mean position. Secondly, during periods of increased low pressure system activity (i.e. the wintertime and high NAO-index periods), the front-related variance is stronger, which is a signature of higher degree of frontal trapping. Thus through theory and observations we have shown that the subsurface part of the ANF and western branch of the NwAC is strongly guided by topography along the Vøring Plateau also on shorter time scales.

Acknowledgements

Many thanks to Svein Østerhus for helping with the OWSM data. Vladimir Borovkov and PINRO (Murmansk) are acknowledged for providing data from the CTD section along 65°45'N. We want to acknowledge met.no (Norwegian Met. office) for providing the Hindcast pressure data and Lars Asplin at IMR for converting it to wind stress fields. The authors are grateful to the anonymous reviewers for their

comments which significantly improved the paper. This work has been partly supported by the Research Council of Norway through the ProClim project, and by the G. C. Rieber Foundations (J.E.Ø.N.). This is publication number A 155 from the Bjerknes Centre for Climate Research.

References

Alekseev, G. V., Johannessen, O. M., Korablev, A. A., Ivanov, V. V., Kovalevski, D. V., 2001. Interannual variability of water mass in the Greenland Sea and the adjacent areas. Polar Research 20 (2), 201–208.

Anderson, D. L. T., Killworth, P. D., 1977. Spin-up of a stratified ocean, with topography. Deep–Sea Research 24 (8), 709–732.

Anon., 1997. Tables with averages of temperature, salinity and normal values in standard sections in the Norwegian and Greenland Seas (1983-1995). Tech. rep., Knipovich Polar Research Institute of Marine Fisheries and Oceanography (PINRO), Murmansk, in russian.

Belkin, I. M., 2004. Propagation of the "Great Salinity Anomaly" of the 1990's around the northern North Atlantic. Geophysical Research Letters 31 (8).

Belkin, I. M., Levitus, S., Antonov, J., Malmberg, S.-A., 1998. "Great Salinity Anomalies" in the North Atlantic. Progress in Oceanography 41 (1), 1–68.

Bjørgen, H., 1971. "Armauer Hansen" ekspedisjonene i Norskehavet 1935 og 1936. Master's thesis, Geophysical Institute, University of Bergen, Allégt.70, 5007 Bergen, Norway.

Blindheim, J., Borovkov, V., Hansen, B., Malmberg, S. A., Turrell, W. R., Østerhus, S., 2000. Upper layer cooling and freshening in the Norwegian Seas in relation to atmospheric forcing. Deep–Sea Research I 47 (4), 655–680.

Blindheim, J., Østerhus, S., 2005. The Nordic Seas, main oceanographic features. In: Drange, H., Dokken, T., Furevik, T., Gerdes, R., Berger, W. (Eds.), The Nordic Seas: An Integrated Perspective. Vol. 158 of Geophysical Monograph Series. American Geophysical Union, Washington DC, pp. 11–38.

Borovkov, V., Krysov, A., 1995. Report from survey of distributions of Norwegian spring spawning herring and environmental conditions in the Norwegian Sea in June-July 1995. In: Report from a Joint Meeting of Russian and Icelandic Scientists in Reykjavik 1995.

Dickson, R., 1972. Variability and continuity within the Atlantic Current of the Norwegian Sea. Rapp. Procès-Verbaux Réunions. Conseil International l'Exploration de la Mer 162, 167–183.

Dickson, R. R., Meincke, J., Malmberg, S.-A., Lee, A. J., 1988. The "Great Salinity Anomaly" in the northern North Atlantic 1968–1982. Progress in Oceanography 20 (2), 103–151.

Furevik, T., Bentsen, M., Drange, H., Johannessen, J. A., Korablev, A., 2002. Temporal and spatial variability of the sea surface salinity in the Nordic Seas. Journal of Geophysical Research 107 (C12).

Gammelsrød, T., Holm, A., 1984. Variations of temperature and saltinity at Station M (66°N 02°E) since 1948. Rapp. Procès-Verbaux Réunions. Conseil International l'Exploration de la Mer 185, 188–200.

Gammelsrød, T., Østerhus, S., Godøy, Ø., 1992. Decadal variations of ocean climate in the Norwegian Sea observed at Ocean Station "Mike" (66°N 2°E). In: Dickson, R., Mälkki, P., G. Radach, R. S., Sissenwine, M. (Eds.), Hydrobiological Variability in the ICES Area, 1980–89. Vol. 195 of ICES Marine Science Symposia. ICES, pp. 68–75.

Hansen, B., Jónsson, S., Turrell, W. R., Østerhus, S., 2000. Seasonal Variations in the Atlantic Water inflow to the Nordic Seas. ICES CM 2000/L 3, 1–15.

Hansen, B., Østerhus, S., 2000. North Atlantic–Nordic Seas exchanges. Progress in Oceanography 45 (2), 109–208.

Heburn, G. W., Johnson, C. D., 1995. Simulations of the mesoscale circulation of the Greenland-Iceland-Norwegian Seas. Journal of Geophysical Research 100 (C3), 4921–4941.

Helland-Hansen, B., 1934. The Sognefjord Section. Oceanographic observations in the northernmost part of the North Sea and the southern part of the Norwegian Sea. In: James Johnstone Memorial Volume. University Press of Liverpool, UK, pp. 257–274.

Helland-Hansen, B., Nansen, F., 1909. The Norwegian Sea: Its Physical Oceanography based upon the Norwegian Researches 1900–1904. Vol. II of Rep. Norw. Fish. Mar. Inv. The Royal Department of Trade, Navigation and Industries, Mallingske, Kristiania, 390 pp.

Hjøllo, S. S., 1999. A comparative study of the Norwegian Sea inflow. Ph.D. thesis, Geophysical Institute, University of Bergen, Allégt.70, 5007 Bergen, Norway.

Johannessen, J. A., Gade, H. G., 1984. A case study of the variations in the upper ocean at Ocean Weather Ship Mike (66°N, 2°E) in the Norwegian Sea. Geophysica Norvegica 32 (5), 165–175.

Jones, P. D., Jonsson, T., Wheeler, D., 1997. Extension to the North Atlantic Oscillation using early instrumental pressure observations from Gibraltar and South-West Iceland. International Journal of Climatology 17 (13), 1433–1450.

Kort, V., Titov, V., Osadchiy, A., 1977. Kinematics and structure of currents in a study area in the Norwegian Sea. Oceanology, English Translation 17 (5), 505–508.

Krauß, W., 1958. Our knowledge about internal waves in the northern North Atlantic Ocean. ICES CM 1958 54, 3 pp.

Kvinge, T., Lee, A., Sætre, R., 1968. Report on study of variability in the Norwegian Sea April/May 1967. Report 15, Geophysical Institute, University of Bergen, Allégt.70, 5007 Bergen, Norway.

Le Floch, J., 1953. Quelques propriétés de la zone de transition entre eau Arctique en Mer de Norvège. Universitetet i Bergen Årbok Matematisk–Naturvitenskapelig Rekke 3, 1–45.

Leinebø, R., 1969. Den Norske Atlanterhavsstrøm. rapport fra målinger høsten 1962. Cruise report, Geophysical Institute, University of Bergen.

Mork, K. A., Blindheim, J., 2000. Variation in the Atlantic Inflow to the Nordic Seas, 1955–1996. Deep–Sea Research I 47 (6), 1035–1057.

Mosby, H., 1950. Recherches océanographiques dans la mer de Norwège a la Station Météorologique M. Cahiers du Centre de Recherches et D'etudes Océanographiques 1, 1–7.

Mosby, H., 1959. Deep water in the Norwegian Sea. Geophysica Norvegica 21 (3),

62 pp.
Mosby, H., 1970. Atlantic Water in the Norwegian Sea. Geophysica Norvegica 28 (1), 60 pp.
Nilsen, F., 2001. On the effect of atmospheric forcing and topography at the Vøring Plateau. Ph.D. thesis, Geophysical Institute, University of Bergen, Allégt.70, 5007 Bergen, Norway.
Nilsen, F., 2004. Forcing of a two-layered water column over a sloping sea floor. Journal of Physical Oceanography 34 (12), 2659–2676.
Nilsen, J. E. Ø., 2003. Variability at Ocean Weather Station M in the Norwegian Sea. In: Turrell, W., Lavín, A., Drinkwater, K. F., St. John, M., Watson, J. (Eds.), Hydrobiological Variability in the ICES Area, 1990–99. Vol. 219 of ICES Marine Science Symposia. ICES, pp. 371–374. *http://www.nersc.no/∼even/doc/thesis/paper1.pdf*
Nilsen, J. E. Ø., Falck, E., 2006. Variations of mixed layer properties in the norwegian sea for the period 1948–1999. Progress in Oceanography 70 (1), 58–90.
Nilsen, J. E. Ø., Gao, Y., Drange, H., Furevik, T., Bentsen, M., 2003. Simulated North Atlantic–Nordic Seas water mass exchanges in an isopycnic coordinate OGCM. Geophysical Research Letters 30 (10).
Nøst, O., Isachsen, P., 2003. The large-scale time-mean ocean circulation in the Nordic Seas and Arctic Ocean estimated from simplified dynamics. Journal of Marine Research 61 (2), 175–210.
Orvik, K. A., Niiler, P., 2002. Major pathways of Atlantic water in the northern North Atlantic and Nordic Seas towards arctic. Geophysical Research Letters 29 (19).
Orvik, K. A., Niiler, P. P., 2001. Circulation of atlantic water in the northern North Atlantic and Nordic Seas. ICES CM 2001/W.
Orvik, K. A., Skagseth, Ø., Mork, M., 2001. Atlantic Inflow to the Nordic Seas. Current structure and volume fluxes from moored current meters, VM–ADCP and SeaSoar-CTD observations, 1995–1999. Deep–Sea Research I 48 (4), 937–957.
Østrem, A. K., 1998. Det intermediære vannet i Norskehavet. Master's thesis, Geophysical Institute, University of Bergen, Allégt.70, 5007 Bergen, Norway.
Poulain, P.-M., Warn-Varnas, A., Niiler, P., 1996. Near surface circulation of the Nordic Seas as measured by lagrangian drifters. Journal of Geophysical Research 101 (C8), 18237–18258.
Read, J., Pollard, R., 1992. Water masses in the region of the Iceland–Færoes Front. Journal of Physical Oceanography 22 (11), 1365–1378.
Rhines, P. B., 1970. Edge-, bottom, and Rossby waves in a rotating stratified fluid. Geophysical Fluid Dynamics 1, 273–302.
Rodionov, V., 1992. On the mesoscale structure of the frontal zones in the Nordic Seas. Journal of Marine Systems 3, 127–139.
Sælen, O. H., 1959. Studies in the Norwegian Atlantic Current. Part I: The Sognefjord Section. Geophysica Norvegica 20 (13), 28 pp.
Sælen, O. H., 1963. Studies in the Norwegian Atlantic Current. Part II: Investigations during the years 1954-59 in an area west of Stad. Geophysica Norvegica 23 (6), 82 pp.
Smart, J. H., 1984. Spatial variability of major frontal systems in the North Atlantic-

Norwegian Sea area: 1980–1981. Journal of Physical Oceanography 14 (1), 185–192.

Svendsen, E., Sætre, R., Mork, M., 1991. Features of the northern North Sea circulation. Continental Shelf Research 11 (5), 493–508.

Swift, J. H., 1986. The arctic waters. In: Hurdle, B. G. (Ed.), The Nordic Seas. Springer Verlag, Ch. 5.

Szczechowoski, C., 1994. A robust technique for computing modal paths for oceanic fronts (abstract). In: Eos Trans. AGU. Vol. 73. p. 148, ocean Sciences Meeting suppl.

Torrence, C., Compo, G. P., 1997. A practical guide to wavelets. Bulletin of the American Meteorological Society 79 (1), 61–78. *http://paos.colorado.edu/research/wavelets*

Willebrand, J., Philander, S., Pacanowski, R., 1980. The oceanic response to large-scale atmospheric disturbances. Journal of Physical Oceanography 10 (3), 411–429.

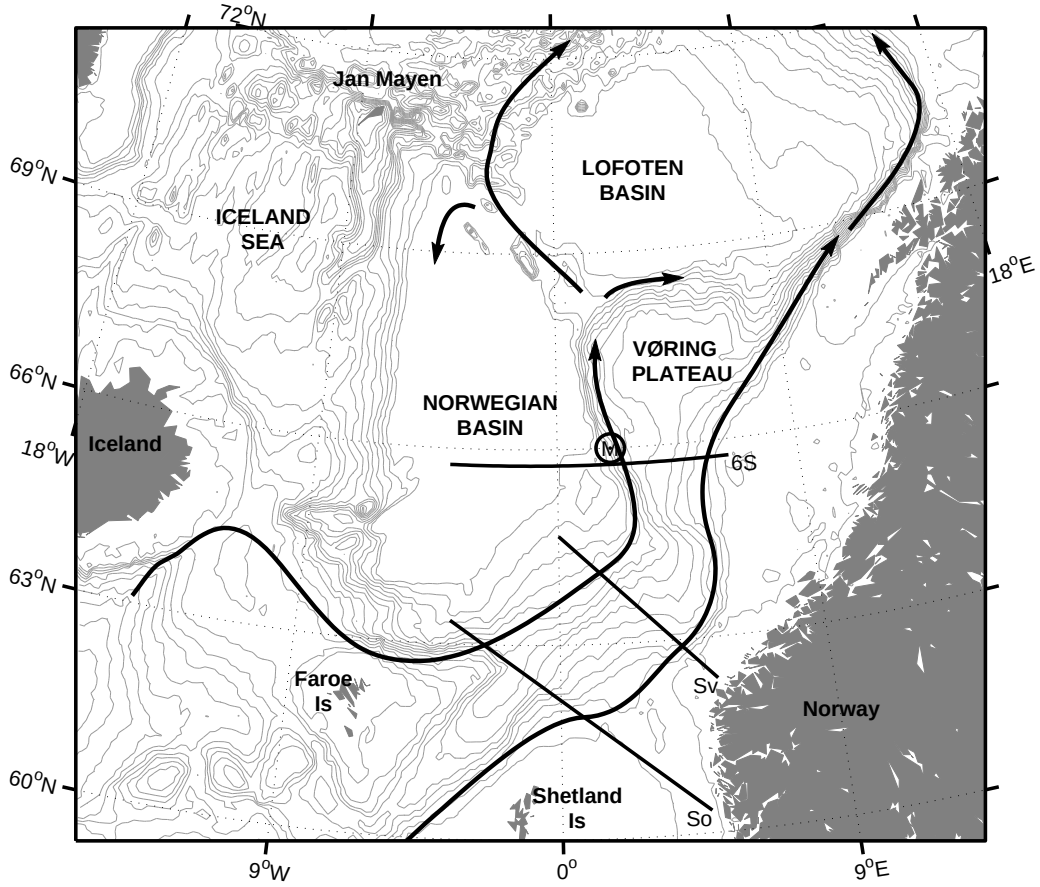

Fig. 1. The Norwegian Basin and adjacent areas. Isobaths are drawn for every 200 m to 3000 m in order to emphasise steep escarpments. Schematic surface currents are based on literature cited in the text. Arrows indicate the two current branches of the Norwegian Atlantic Current: An eastern barotropic flow following the Norwegian continental slope, and a western baroclinic jet following the Atlantic Norwegian Front as a continuation of the Faroe Current along the Iceland Faroe Front. Marked lines indicate the Russian (6S), Svinøy (Sv), and Sognefjord (So) Section. Circled M indicates the position of Ocean Weather Station M.

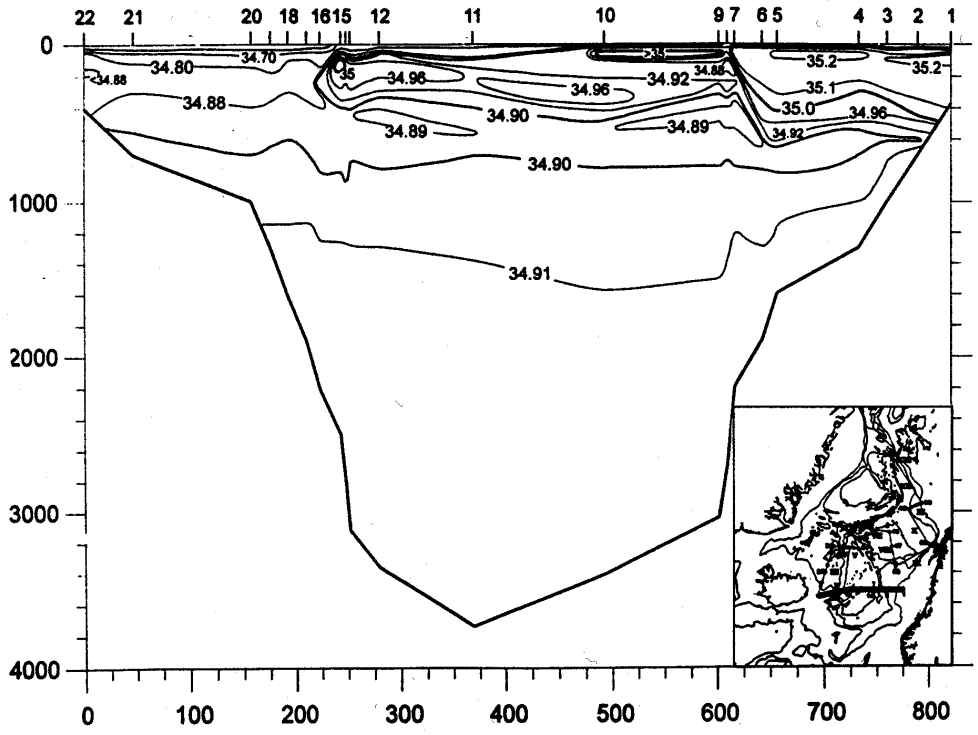

Fig. 2. Salinity section across the Norwegian Sea between Norway and Iceland from a R/V Håkon Mosby cruise in August 1994. From Østrem (1998).

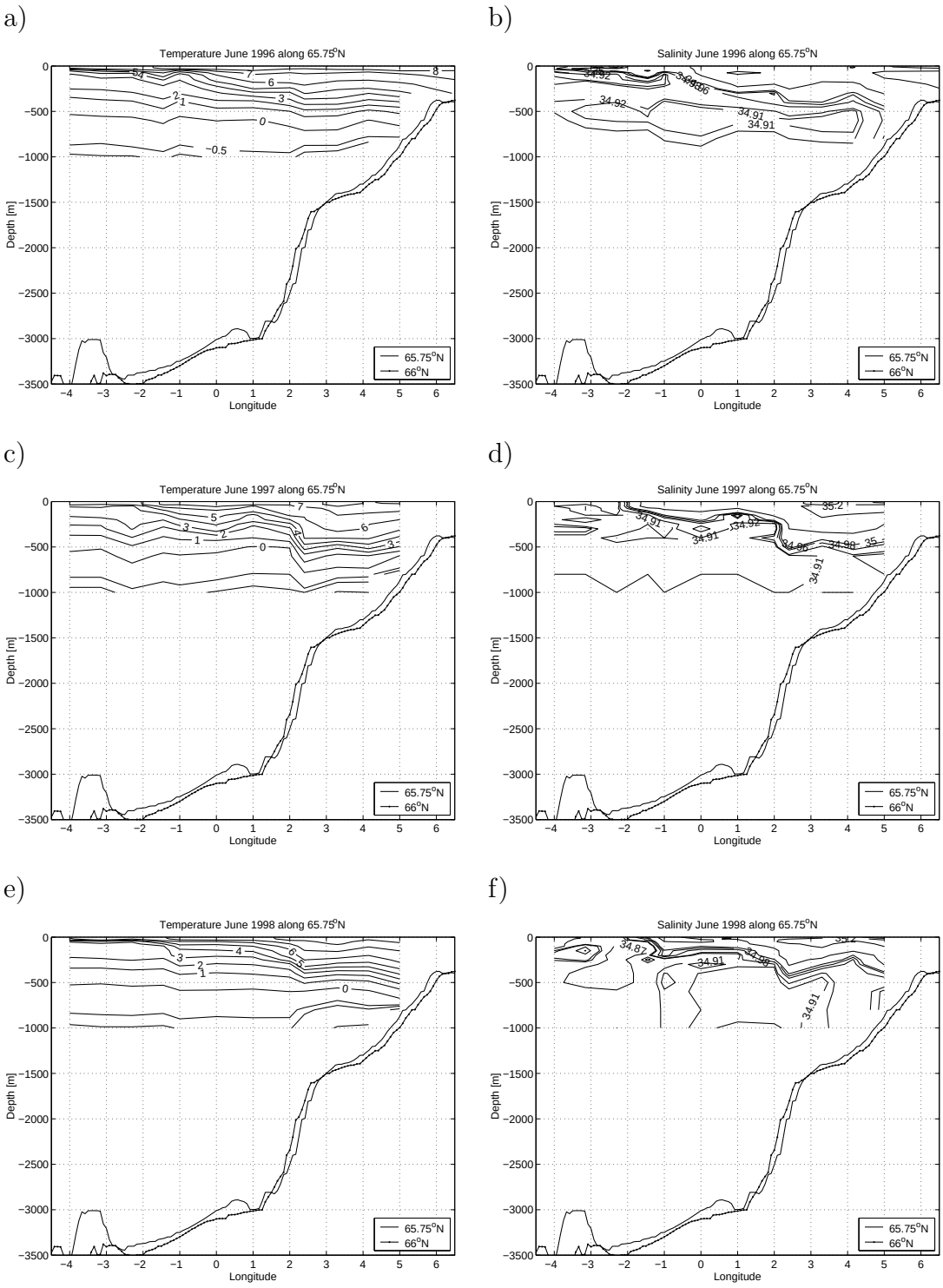

Fig. 3. Temperature (left) and salinity (right) in the Russian standard section along 65°45'N (6S; Borovkov and Krysov, 1995), which has been worked every June since 1963 (See Figure 1). The hydrographic section data from June 1996 (a,b), 1997 (c,d) and 1998 (e,f) was provided by PINRO, Murmansk.

a)

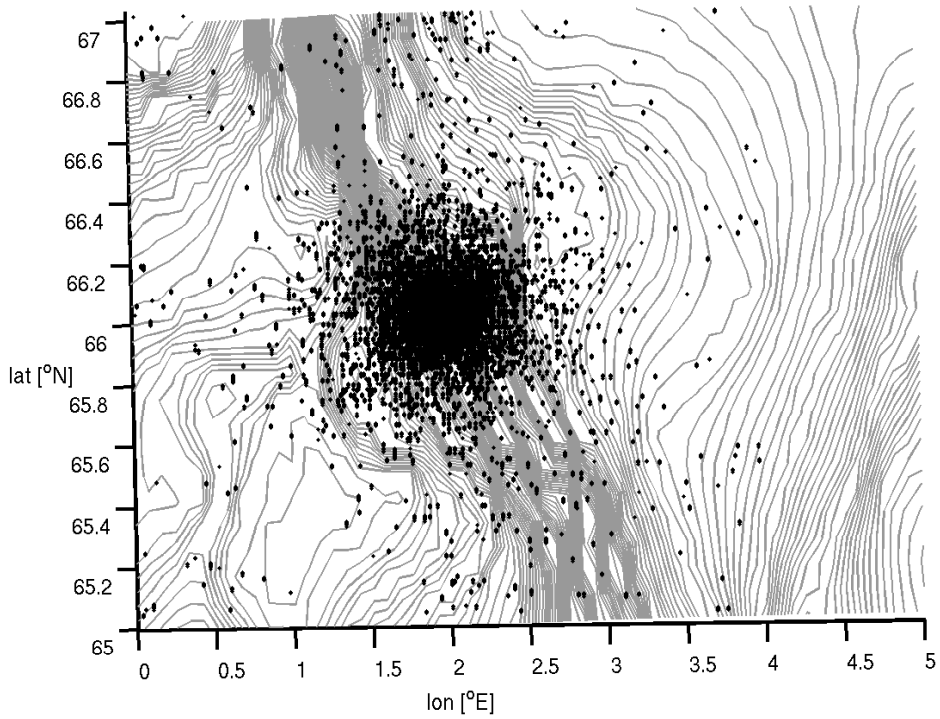

b)

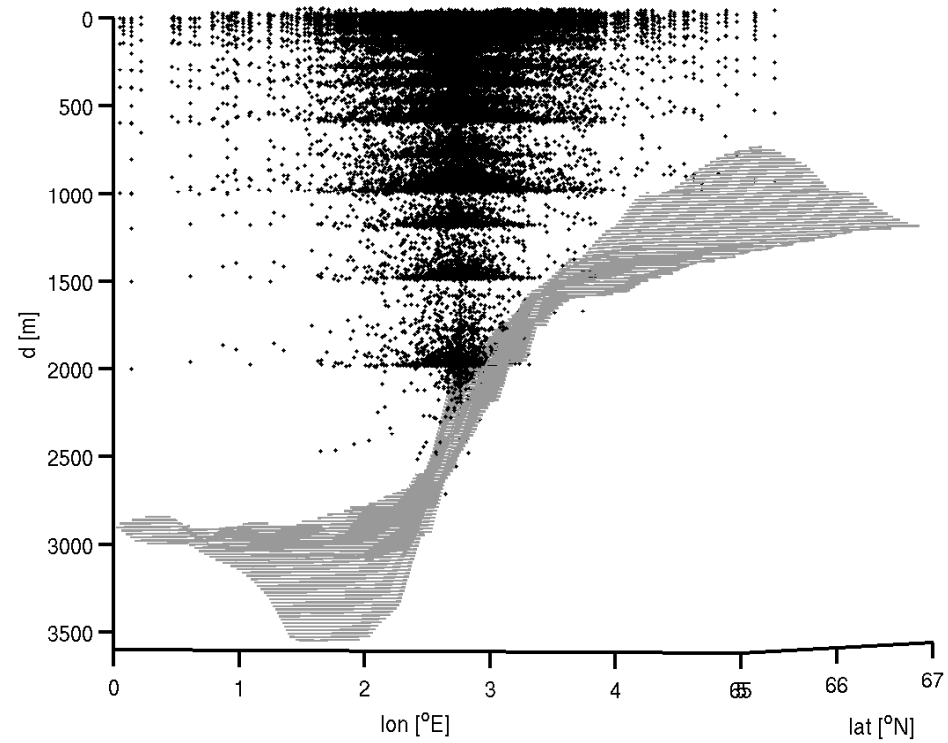

Fig. 4. The data samples in space, horizontal (a) and vertical (b) distribution. Gray lines represent isobaths. The axes in (b) are rotated for an along slope perspective.

a)

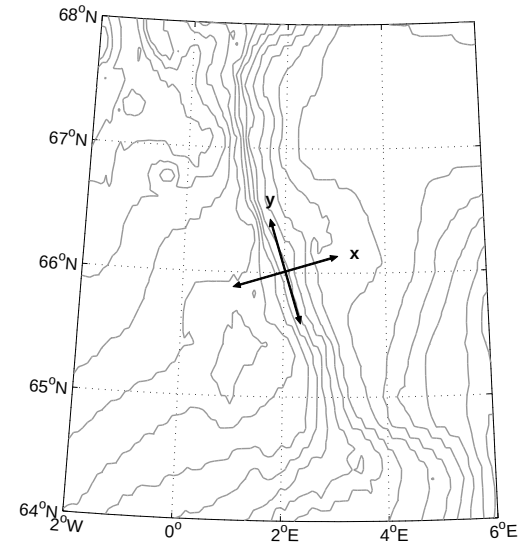

b)

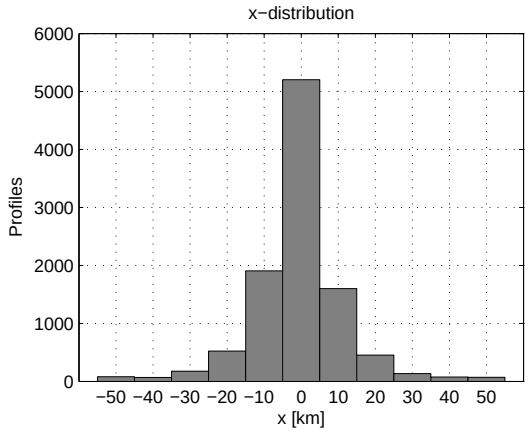

c)

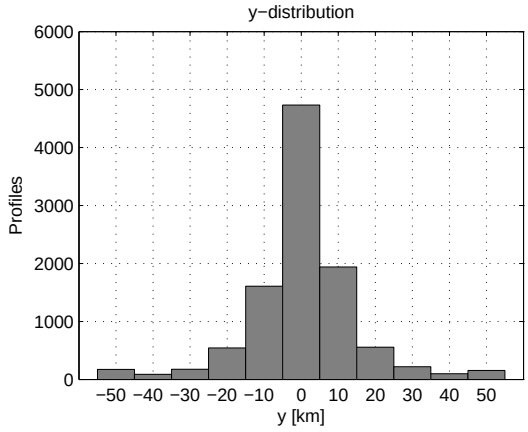

Fig. 5. a) The Cartesian coordinate-system used in this study. The y-axis is aligned along the bottom slope, with positive direction northward. The length of the arrows is approximately 50 km. Panels b) and c) show distribution of measurements along the two axes.

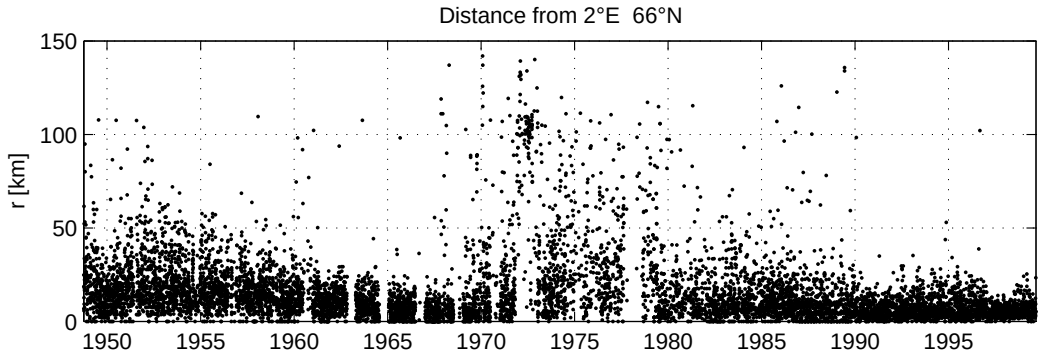

Fig. 6. Time series of deviation from designated position.

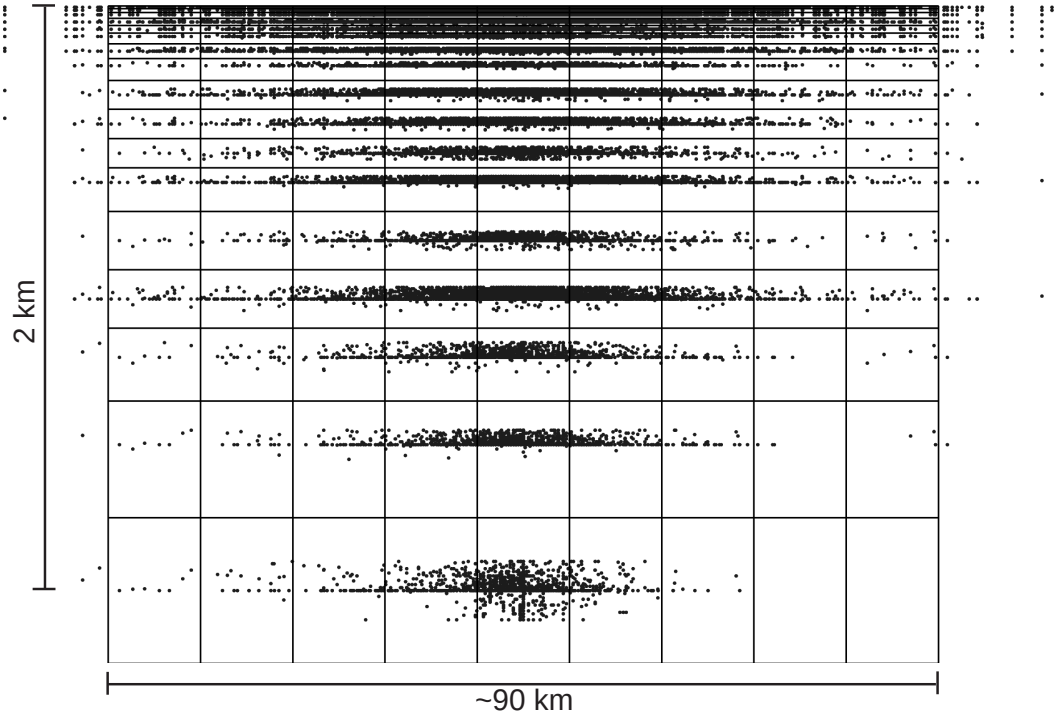

Fig. 7. The bins in which mean values are calculated. Nine 10 km wide bins laterally (x-axis) and 17 bins centred on the standard depths (0–2000 m, y-axis).

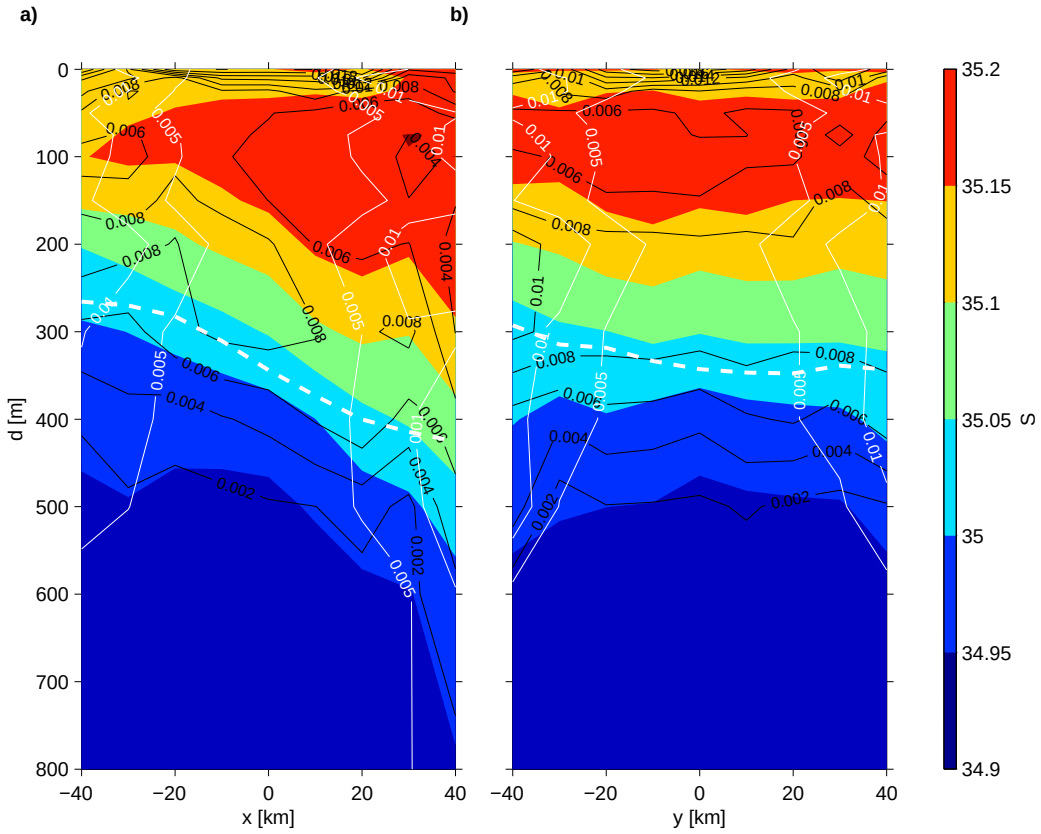

Fig. 8. The mean (1948–99) section of salinity across (a) and along (b) the bottom slope. Black contour lines indicates variance in the bins. Whole white contour lines indicate error estimate for the bin mean values, with contours chosen at 1/10 and 2/10 of the contour steps for the water property. Dashed white lines indicate the σ_t=27.8 isopycnal found from mean sections of density anomaly (Figure 10).

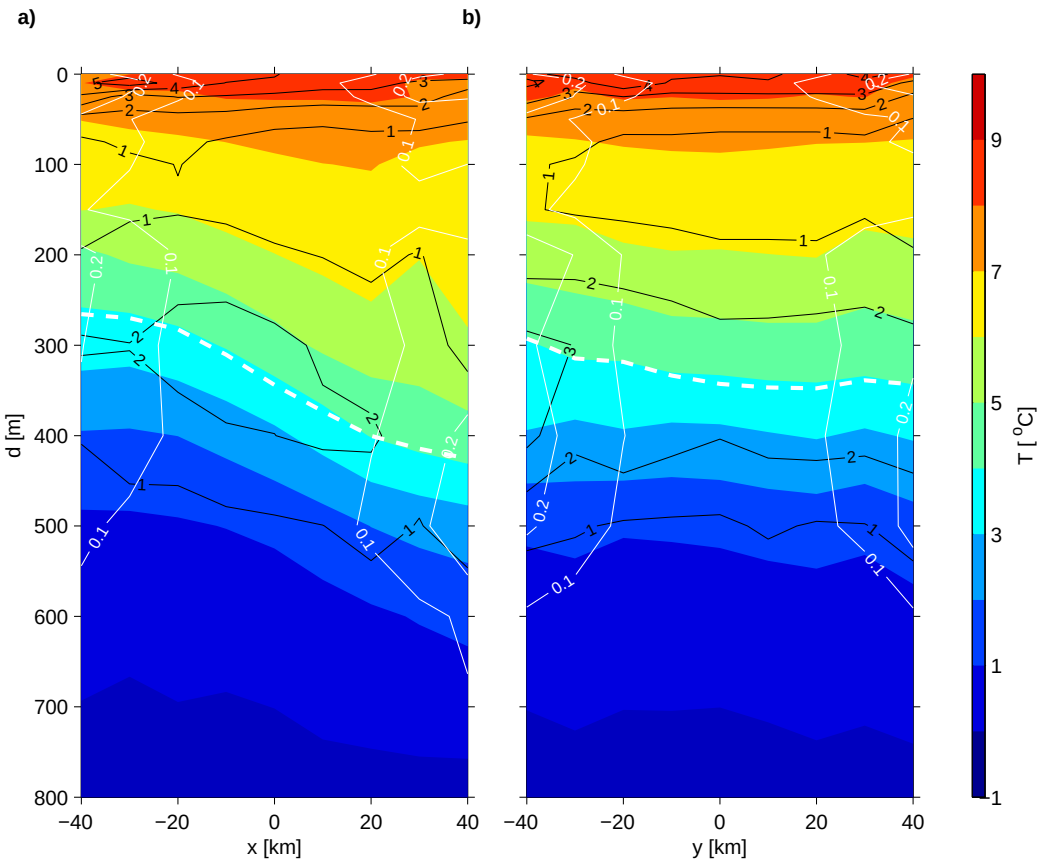

Fig. 9. The mean (1948–99) temperature section. Details as in Figure 8.

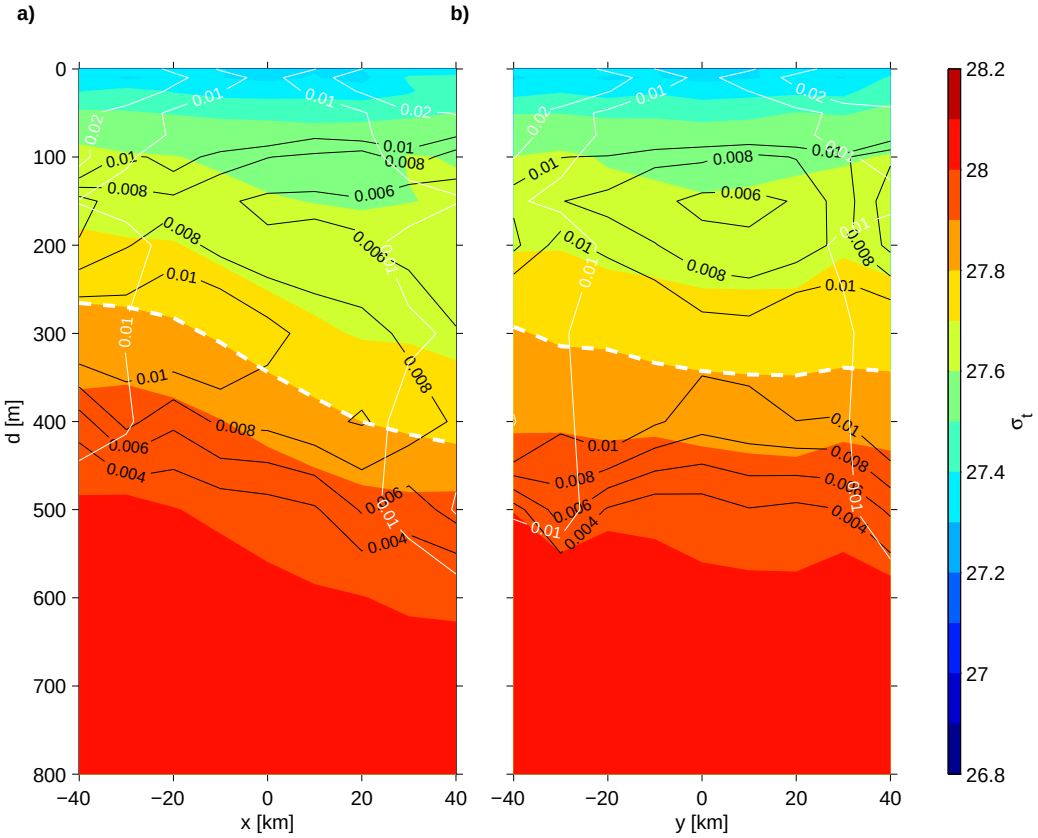

Fig. 10. The mean (1948–99) density section. Details as in Figure 8.

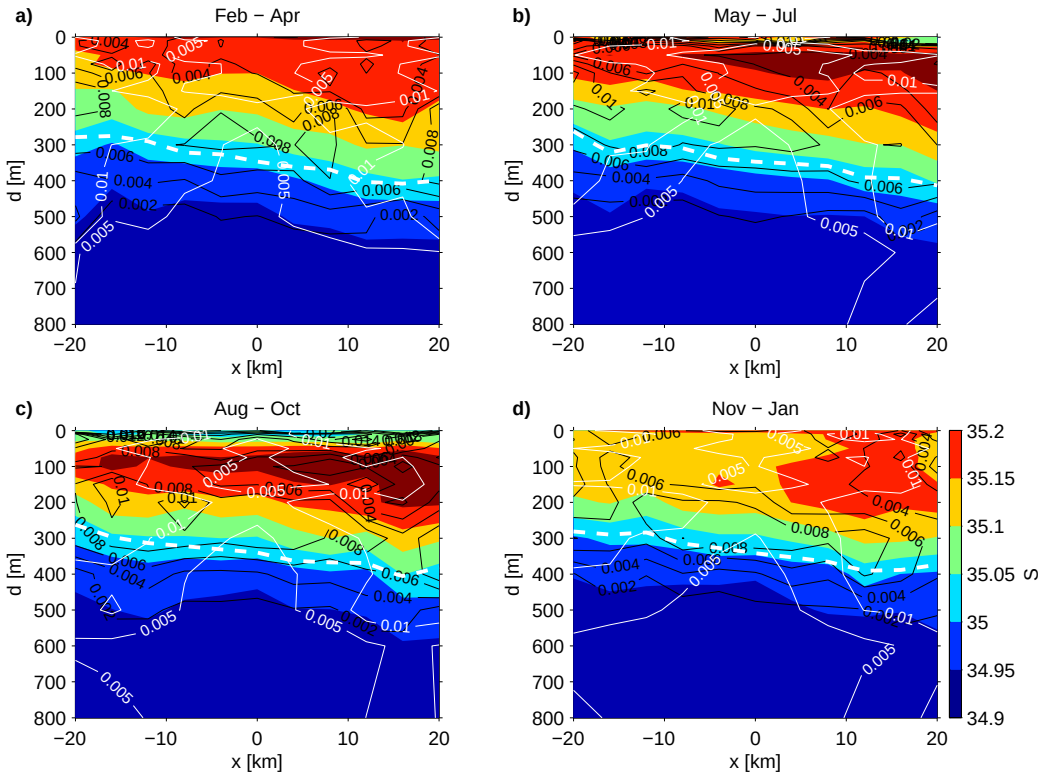

Fig. 11. Cross slope salinity distribution in four seasons. Dashed white lines indicate the σ_t=27.8 isopycnal found from seasonal sections of density anomaly (Figure 13). Other details as in Figure 8.

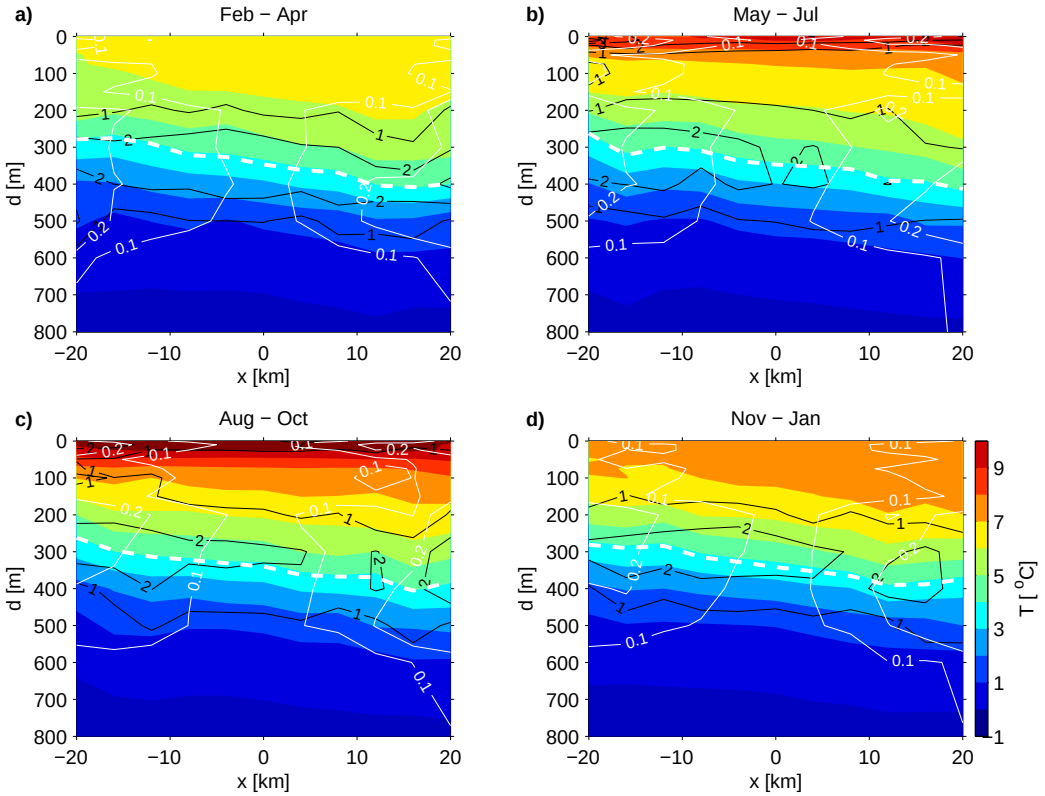

Fig. 12. Cross slope temperature distribution in four seasons. Details as in Figure 11.

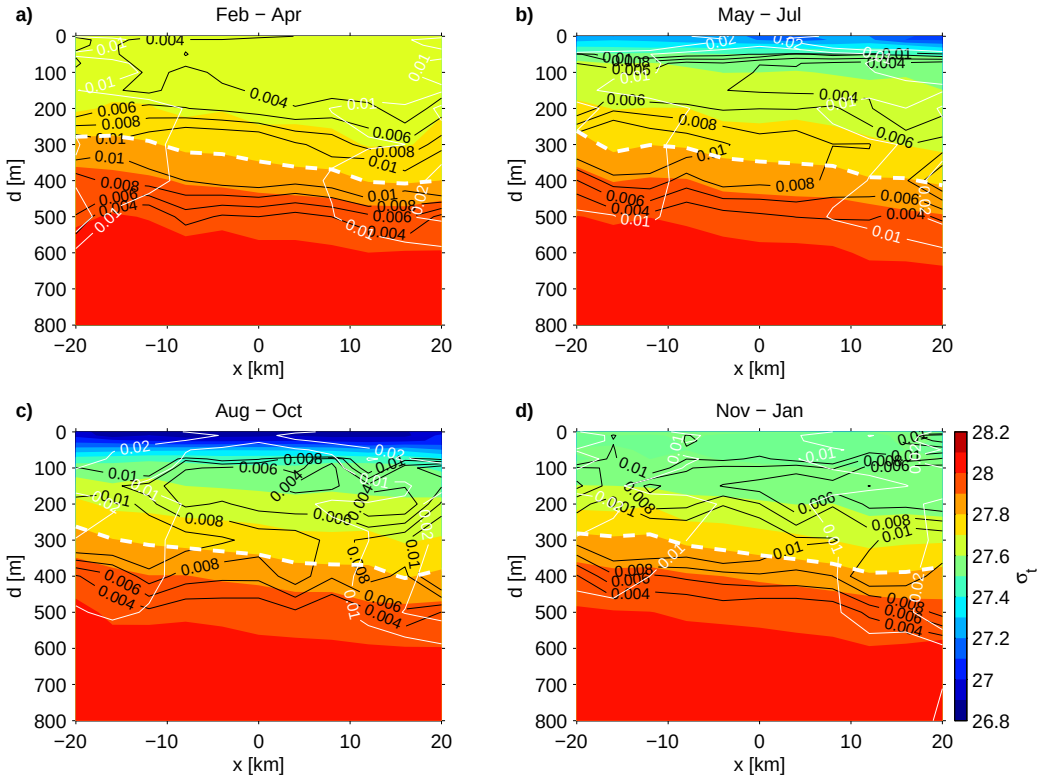

Fig. 13. Cross slope density distribution in four seasons. Details as in Figure 11.

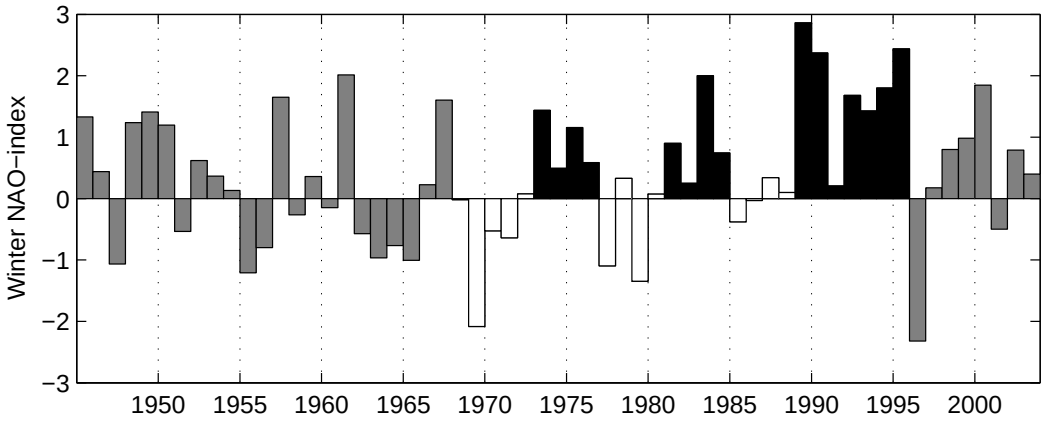

Fig. 14. The North Atlantic Oscillation (NAO) winter index (December to March mean) as defined by Jones et al. (1997). In the winter, the difference between the normalized sea level pressure over Gibraltar and the normalized sea level pressure over Southwest Iceland is a useful index of the strength of the prevailing westerly winds in the North Atlantic. Three consecutive periods with relatively high NAO-index (black bars) and weak or negative (white bars) are used for composite studies here.

a)

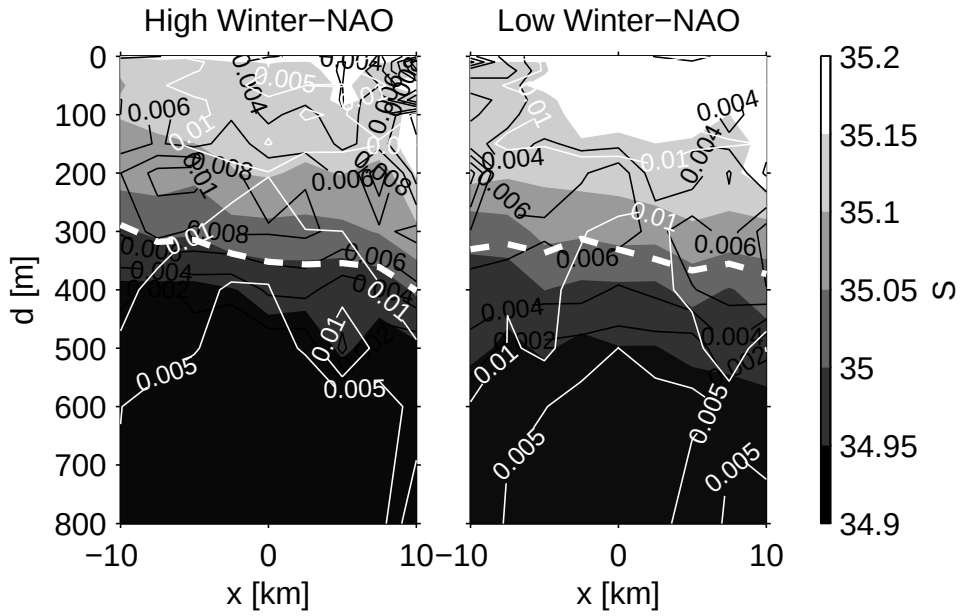

b)

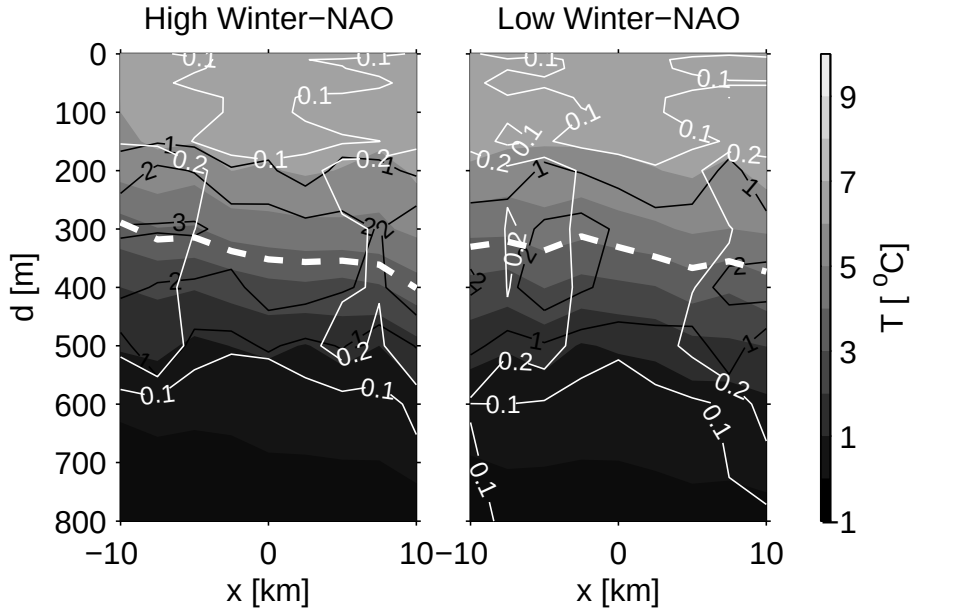

Fig. 15. The mean cross-slope sections of salinity (a) and temperature (b) from high and low NAO-index winters. Dashed white lines indicate the σ_t=27.8 isopycnal found from corresponding sections of density anomaly (not shown). Other details as in Figure 8.

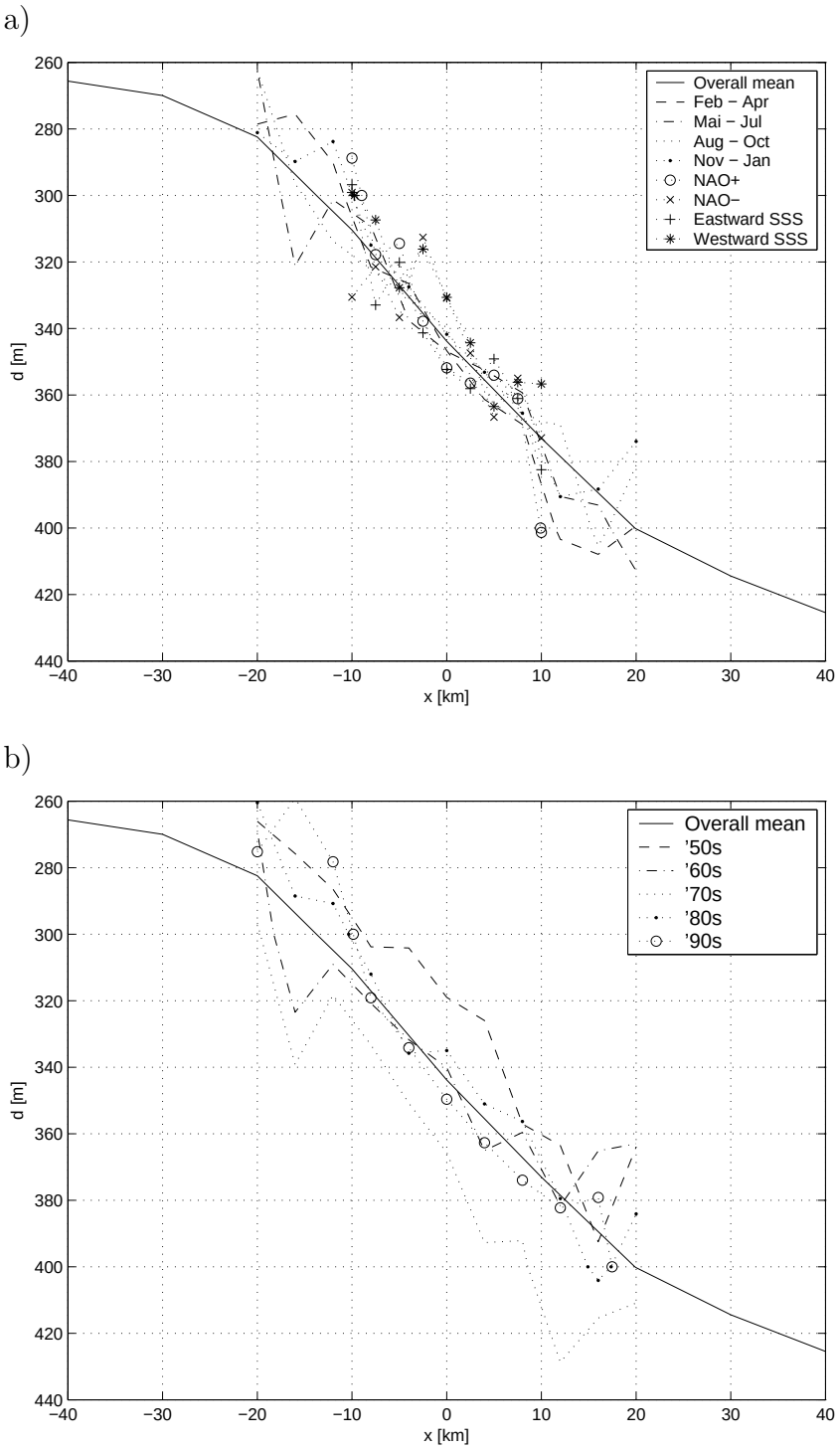

Fig. 16. Cross slope depth of the σ_t=27.8 isopycnal representing the pycnocline at OWSM, for different situations (composite studies) (a) and for the different decades (b).

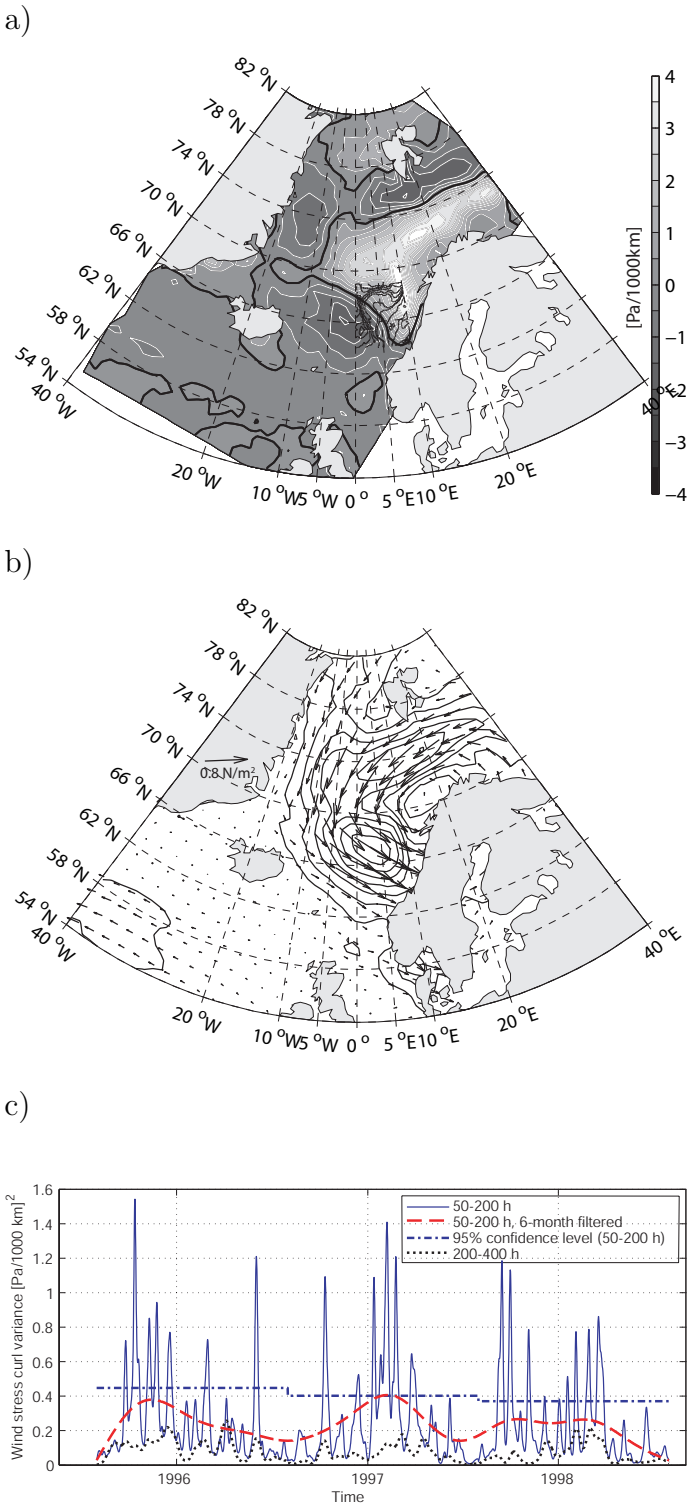

Fig. 17. The wind stress curl (a) calculated from the wind stress vectors (b) over the Nordic Seas and the Barents Sea. Thick black contour in (a) represents zero wind stress curl and the Vøring Plateau is outlined by black isobaths. Contours in (b) indicate the absolute wind stress. The wind stress field is a 24-hour average from May 2nd, 1997. In (c) the 3-year time series of the scale-averaged wavelet power of wind stress curl using a Morlet mother wavelet (Torrence and Compo, 1997), for the period band between 50–200 h (thin line) and 200–400 h (dotted line) is shown. For the 50–200 h band, 6-month running mean filtered series (dashed line) and annual estimates of the 95% confidence interval (dot-dashed line) are also drawn.

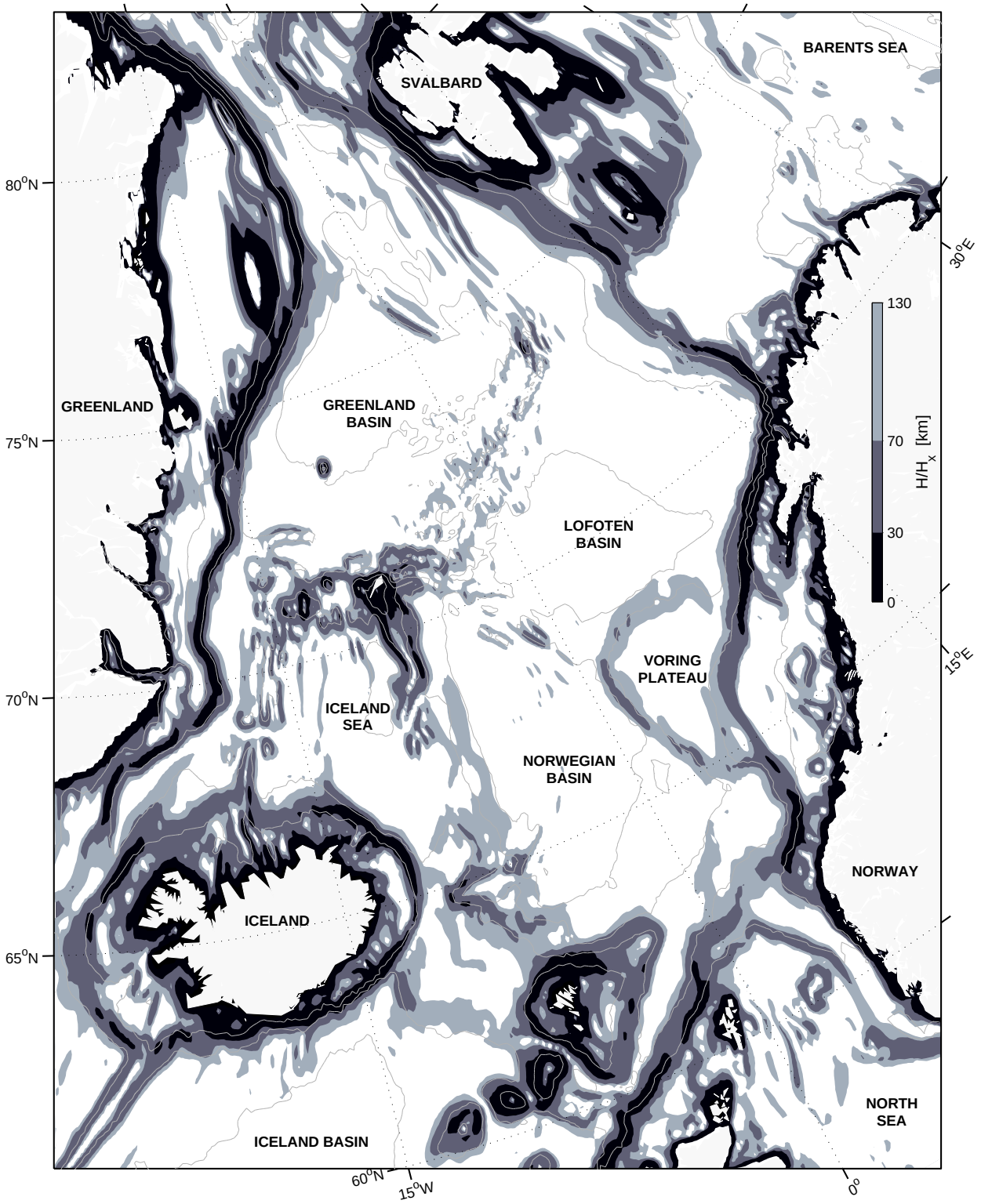

Fig. 18. Values of $\frac{H}{H_x}$ based on the ETOPO5 bathymetry data (black and greyscale patches), showing where in the Nordic Seas and adjacent areas there most likely will exist topographically trapped waves and what their horizontal scales will be. The x-direction is across slope. White areas have weak or no slope and thus values above scale. Grey isobaths at 300, 1000, 2000, and 3000 m are drawn for geographical guidance.